Thick Shell Element Form 5 in LS-DYNA

Lee P. Bindeman
Livermore Software Technology Corporation

Thick shell form 5 in LS-DYNA is a layered 8 node brick element, with 4 nodes defining the bottom surface and 4 defining the top. For computational efficiency, each layer has one in-plane integration point. At least 2 layers are needed through the thickness, but there is no limit to the number of layers that may be defined.

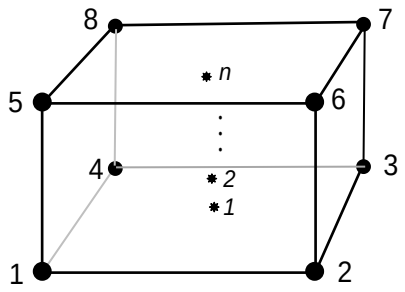

Fig. 1.1 Thick shell element form 5 with n integration points.

The through-thickness orientation of the integration points gives the element the ability to capture bending like a plate or shell element, but it can also capture the thickness stress like a brick element. Like brick element form 1, thick shell form 5 is based on the trilinear shape functions.

Before describing how the strain is evaluated, it is useful to introduce two coordinate systems, one being a corotational system ($\hat{x}$, $\hat{y}$, $\hat{z}$), and the second a referential coordinates system (x, h, z). The map to the corotational system is a simple rotation from the global coordinate system. The corotational system has its origin at the element centroid, and is defined by vectors that pass through the centers of opposite faces. For skewed elements, the corotational system is orthogonalized and may not pass exactly through face centers. In the referential system, the element is a cube with edge lengths of 2. The origin of the referential system is at the center and the axes intersect the element faces at -1 and

+1.

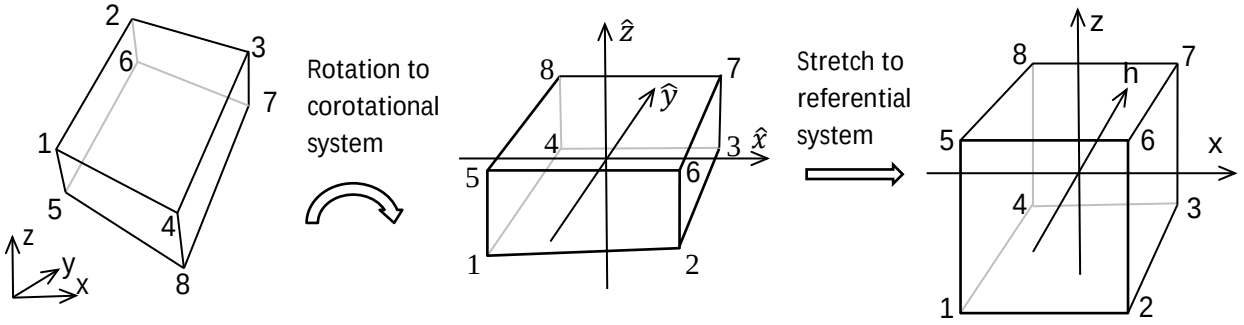

Fig. 1.2 Element geometry in global, corotational, and referential coordinate systems

In the referential system, we can evaluate a variable at any location within the element in terms of nodal values, $\boldsymbol{u}_I$, using the trilinear shape functions as shown in Eq. 1.1.

$$\boldsymbol{u}(\xi,\eta,\zeta) = N_I(\xi,\eta,\zeta)u_I \qquad \text{Eq. 1.1}$$

In Eq. 1.1 and those that follow, the upper case subscript, I, refers to node numbers 1 to 8, and the repeated subscript indicates a summation from 1 to 8. Below, lower case subscripts will refer to the spatial coordinates, 1 to 3. The well-known trilinear shape functions can be written at each node in terms of the referential coordinates, and the value of the referential coordinates at the node, either +1 or -1.

$$N_I(\xi,\eta,\zeta) = \frac{1}{8}(1+\xi_I\xi)(1+\eta_I\eta)(1+\zeta_I\zeta) \qquad \text{Eq. 1.2}$$

The development of a strain field follows the development for the 1-point brick element in Belytschko and Bindeman, 1993, where it was shown that the displacement or velocity field could be written in terms of the shape function derivatives, $\boldsymbol{b}$, orthogonal gamma vectors of Belytschko, Ong, Liu, and Kennedy, 1984, and the nodal values of displacements or velocities, $\boldsymbol{v}_i$.

$$v_i = a_{0i} + \left(x\boldsymbol{b}_x^t + y\boldsymbol{b}_y^t + z\boldsymbol{b}_z^t + h_1\boldsymbol{\gamma}_1^t + h_2\boldsymbol{\gamma}_2^t + h_3\boldsymbol{\gamma}_3^t + h_4\boldsymbol{\gamma}_4^t\right)\boldsymbol{v}_i \qquad \text{Eq. 1.3}$$

$$\widehat{\boldsymbol{b}}_x^t = \frac{1}{V}\int_{\Omega_e}\frac{\partial \boldsymbol{N}(\xi,\eta,\zeta)}{\partial x}d\Omega \qquad \text{Eq. 1.4}$$

$$\widehat{\boldsymbol{\gamma}}_\alpha = \frac{1}{8}\left[\boldsymbol{h}_\alpha - \sum_{j=1}^{3}\left(\boldsymbol{h}_\alpha^t\boldsymbol{x}_j\right)\widehat{\boldsymbol{b}}_j\right] \qquad \text{Eq. 1.5}$$

In Eq. 1.3, h_1 to h_4 are defined in terms of the referential coordinates.

$$h_1 \equiv \eta\zeta \qquad h_2 \equiv \zeta\xi \qquad h_3 \equiv \xi\eta \qquad h_4 \equiv \xi\eta\zeta \qquad \text{Eq. 1.6}$$

In Eq. 1.4, the integral is over the element domain, and closed form expressions are in terms of nodal coordinates are presented in Belytschko et al., 1984. In Eq. 1.7, the expressions for h_1 to h_4 have been evaluated at the 8 nodes to create 8x1 arrays of +1 and -1.

$$\begin{aligned}\boldsymbol{h}_1^t &\equiv (+1,+1,-1,-1,-1,-1,+1,+1)\\ \boldsymbol{h}_2^t &\equiv (+1,-1,-1,+1,-1,+1,+1,-1)\\ \boldsymbol{h}_3^t &\equiv (+1,-1,+1,-1,+1,-1,+1,-1)\\ \boldsymbol{h}_4^t &\equiv (-1,+1,-1,+1,+1,-1,+1,-1)\end{aligned} \qquad \text{Eq. 1.7}$$

Using Eq. 1.3 with nodal velocities, $\boldsymbol{v}_I$, and taking the derivative with respect to the corotational coordinates, we get terms of the spatial gradient of velocity, $\boldsymbol{L}$.

$$L_{ij} = \frac{\partial v_i}{\partial \hat{x}_j} = \sum_{I=1}^{8} \frac{\partial N_I}{\partial x_j} v_{iI} = \left(\widehat{\boldsymbol{b}}_j^t + h_{\alpha,j}\widehat{\boldsymbol{\gamma}}_\alpha^t\right)\boldsymbol{v}_i \qquad \text{Eq. 1.8}$$

The strain measure of the element will be calculated from the rate-of-deformation, $\boldsymbol{D}$ which is the symmetric part of $\boldsymbol{L}$. If the 6 unique terms of the rate-of-deformation are arranged in a 6x1 array, then the calculation of them can be written as a matrix multiplication.

$$\begin{Bmatrix} D_{11}\\ D_{22}\\ D_{33}\\ D_{12}\\ D_{13}\\ D_{23}\end{Bmatrix} = \begin{bmatrix} \widehat{\boldsymbol{b}}_x^t + h_{\alpha,x}\widehat{\boldsymbol{\gamma}}_\alpha^t & 0 & 0\\ 0 & \widehat{\boldsymbol{b}}_y^t + h_{\alpha,y}\widehat{\boldsymbol{\gamma}}_\alpha^t & 0\\ 0 & 0 & \widehat{\boldsymbol{b}}_z^t + h_{\alpha,z}\widehat{\boldsymbol{\gamma}}_\alpha^t\\ \widehat{\boldsymbol{b}}_y^t + h_{\alpha,y}\widehat{\boldsymbol{\gamma}}_\alpha^t & \widehat{\boldsymbol{b}}_x^t + h_{\alpha,x}\widehat{\boldsymbol{\gamma}}_\alpha^t & 0\\ \widehat{\boldsymbol{b}}_z^t + h_{\alpha,z}\widehat{\boldsymbol{\gamma}}_\alpha^t & 0 & \widehat{\boldsymbol{b}}_x^t + h_{\alpha,x}\widehat{\boldsymbol{\gamma}}_\alpha^t\\ 0 & \widehat{\boldsymbol{b}}_z^t + h_{\alpha,z}\widehat{\boldsymbol{\gamma}}_\alpha^t & \widehat{\boldsymbol{b}}_y^t + h_{\alpha,y}\widehat{\boldsymbol{\gamma}}_\alpha^t \end{bmatrix} \cdot \begin{Bmatrix} \boldsymbol{v}_x\\ \boldsymbol{v}_y\\ \boldsymbol{v}_z\end{Bmatrix} \qquad \text{Eq. 1.9}$$

Eq. 1.9, $\boldsymbol{b}_i^t$ and $\boldsymbol{\gamma}_x^t$ are 1x8 arrays of nodal values, and $\boldsymbol{v}_i$ is a 8x1 array of nodal velocities. The repeated alpha subscripts on *h* and $\boldsymbol{g}$indicate a summation from 1 to 4. Calling the matrix with the $\boldsymbol{b}_i^t$ and $\boldsymbol{\gamma}_x^t$ terms $\boldsymbol{B}$, we can write the Eq. 1.9 as a matrix multiplication.

$$\boldsymbol{D} = \boldsymbol{B} \cdot \boldsymbol{v} \qquad \text{Eq. 1.10}$$

To be correct, the bottom 3 rows of $\boldsymbol{B}$ should be scaled by ½, but omitting this should not cause confusion and simplifies the equations.

Eq. 1.9 is gives the rate of deformation that is consistent with the trilinear shape functions. If this was used as a strain measure for the element, it would exhibit volumetric locking and excessive shear stiffness. Modifications to the B matrix were made in Belytschko and Bindeman, 1993, to correct these problems in a 1-point brick based on the QBI assumed strain field where QBI is an acronym for quintessential bending incompressible. Thick shell form 5 also uses the QBI assumptions, not only for hourglass control, but also to modify the strain rate at the integration points to achieve element stress with the same beneficial properties. Because thick shell form 5 is a layered element, it can achieve accurate coarse mesh results with nonlinear material models as well as the linear solutions that the brick can achieve.

To prevent locking in incompressible materials, the QBI strain field adds terms in the upper half of the matrix to approximate Poisson's effects. It also removes terms from the bottom half to prevent excessive shear stiffness during bending. This shear correction is consistent with assuming the top and

bottom surface of the element is curved during bending so that there is no shear stress during pure bending.

To simplify equations, we introduce notation with up to four subscripts that indicate which terms of the summation are retained, and $\boldsymbol{X}$, $\boldsymbol{Y}$, or $\boldsymbol{Z}$ is used to indicate the variable for the partial derivative. Examples of this notation are shown in Eqs. 1.11.

$$\widehat{\boldsymbol{X}}_{1234} \equiv \sum_{\alpha=1}^{4} h_{\alpha,x}\widehat{\boldsymbol{\gamma}}_{\alpha}^{t} \qquad \widehat{\boldsymbol{Y}}_{1234} \equiv \sum_{\alpha=1}^{4} h_{\alpha,y}\widehat{\boldsymbol{\gamma}}_{\alpha}^{t} \qquad \widehat{\boldsymbol{Z}}_{1234} \equiv \sum_{\alpha=1}^{4} h_{\alpha,z}\widehat{\boldsymbol{\gamma}}_{\alpha}^{t} \qquad \text{Eq. 1.11}$$

$$\widehat{\boldsymbol{X}}_{14} \equiv h_{1,x}\widehat{\boldsymbol{\gamma}}_{1}^{t} + h_{4,x}\widehat{\boldsymbol{\gamma}}_{4}^{t} \qquad \widehat{\boldsymbol{Y}}_{12} \equiv h_{1,y}\widehat{\boldsymbol{\gamma}}_{1}^{t} + h_{2,y}\widehat{\boldsymbol{\gamma}}_{2}^{t}$$

Using Eqs. 1.10, the $\boldsymbol{B}$ matrix for the QBI assumed strain is shown in Eq. 1.11.

$$\boldsymbol{B} = \begin{bmatrix} \widehat{\boldsymbol{b}}_{x}^{t} + \widehat{\boldsymbol{X}}_{1234}^{t} & -\bar{\nu}\widehat{\boldsymbol{Y}}_{3}^{t} - \nu\widehat{\boldsymbol{Y}}_{24}^{t} & -\bar{\nu}\widehat{\boldsymbol{Z}}_{2}^{t} - \nu\widehat{\boldsymbol{Z}}_{34}^{t} \\ -\bar{\nu}\widehat{\boldsymbol{X}}_{3}^{t} - \nu\widehat{\boldsymbol{X}}_{14}^{t} & \widehat{\boldsymbol{b}}_{y}^{t} + \widehat{\boldsymbol{Y}}_{1234}^{t} & -\bar{\nu}\widehat{\boldsymbol{Z}}_{1}^{t} - \nu\widehat{\boldsymbol{Z}}_{34}^{t} \\ -\bar{\nu}\widehat{\boldsymbol{X}}_{2}^{t} - \nu\widehat{\boldsymbol{X}}_{14}^{t} & -\bar{\nu}\widehat{\boldsymbol{Y}}_{1}^{t} - \nu\widehat{\boldsymbol{Y}}_{24}^{t} & \widehat{\boldsymbol{b}}_{z}^{t} + \widehat{\boldsymbol{Z}}_{1234}^{t} \\ \widehat{\boldsymbol{b}}_{y}^{t} + \widehat{\boldsymbol{Y}}_{12}^{t} & \widehat{\boldsymbol{b}}_{x}^{t} + \widehat{\boldsymbol{X}}_{12}^{t} & 0 \\ \widehat{\boldsymbol{b}}_{z}^{t} + \widehat{\boldsymbol{Z}}_{13}^{t} & 0 & \widehat{\boldsymbol{b}}_{x}^{t} + \widehat{\boldsymbol{X}}_{13}^{t} \\ 0 & \widehat{\boldsymbol{b}}_{z}^{t} + \widehat{\boldsymbol{Z}}_{23}^{t} & \widehat{\boldsymbol{b}}_{y}^{t} + \widehat{\boldsymbol{Y}}_{23}^{t} \end{bmatrix} \qquad \text{Eq. 1.12}$$

Because the corotational coordinate system and the referential coordinate system area aligned, we can make the simplifying assumptions in Eq. 1.13. For skewed elements, Eqs. 1.13 are only approximate, but Belytschko and Bindeman, 1993, concluded that the assumptions do not affect element behavior.

$$\frac{\partial \xi_i}{\partial \hat{x}_i} = \frac{1}{\partial \hat{x}_i / \partial \xi_i} = \frac{1}{\frac{1}{8}(\boldsymbol{\Lambda}_i^t \hat{\boldsymbol{x}}_i)} \qquad \frac{\partial \xi_i}{\partial \hat{x}_j} = 0 \text{ for } i \neq j \qquad \text{Eq. 1.13}$$

In Eq. 1.13, the $\boldsymbol{\Lambda}$ terms are 8x1 arrays of +1 and -1 what that represent the stretching modes in the referential system.

$$\boldsymbol{\Lambda}_1^t \equiv (-1, +1, +1, -1, -1, +1, +1, -1)$$

$$\boldsymbol{\Lambda}_2^t \equiv (-1, -1, +1, +1, -1, -1, +1, +1)$$

$$\boldsymbol{\Lambda}_3^t \equiv (-1, -1, -1, -1, +1, +1, +1, +1)$$

With Eq. 1.13, and the fact that ξ=0 and η = 0 for all integration points, we can consider the partial derivatives of h_1 to h_4 from Eq. 1.6. There are some terms that will be zero throughout the element domain because the partial derivatives are everywhere zero. Others will be non-zero throughout most of the element domain. A third type will be zero at the integration points, but nonzero elsewhere in the element domain. Examples of the 3 types are shown in Eqs. 1.15 to 1.17.

$$\frac{\partial h_1}{\partial x} = \frac{\partial \eta}{\partial x}\zeta + \eta\frac{\partial \zeta}{\partial x} = 0 \text{ everywhere} \qquad \text{Eq. 1.15}$$

$$\frac{\partial h_1}{\partial y} = \frac{\partial \eta}{\partial y}\zeta + \eta\frac{\partial \zeta}{\partial y} \neq 0 \text{ everywhere except } \zeta = 0 \qquad \text{Eq. 1.16}$$

$$\frac{\partial h_1}{\partial z} = \frac{\partial \eta}{\partial z}\zeta + \eta\frac{\partial \zeta}{\partial z} = 0 \text{ at integration points but nonzero where } \eta \neq 0 \qquad \text{Eq. 1.17}$$

We can omit the first type from $\boldsymbol{B}$ because they do not contribute anything. The second type will be included in the calculation of strain. The third type will used in the hourglass control. We can then split $\boldsymbol{B}$ into 2 parts, $\overline{\boldsymbol{B}}$ which will generate strain at the integration points and is passed to the stress update routine, and $\widetilde{\boldsymbol{B}}$ which will be used to construct hourglass control.

$$\boldsymbol{B} = \overline{\boldsymbol{B}} + \widetilde{\boldsymbol{B}} \qquad \text{Eq. 1.18}$$

$$\overline{\boldsymbol{B}} = \begin{bmatrix} \widehat{\boldsymbol{b}}_x^t + \widehat{\boldsymbol{X}}_2^t & \mathbf{0} & \mathbf{0} \\ \mathbf{0} & \widehat{\boldsymbol{b}}_y^t + \widehat{\boldsymbol{Y}}_1^t & \mathbf{0} \\ -\bar{\nu}\widehat{\boldsymbol{X}}_2^t & -\bar{\nu}\widehat{\boldsymbol{Y}}_1^t & \widehat{\boldsymbol{b}}_z^t \\ \widehat{\boldsymbol{b}}_y^t + \widehat{\boldsymbol{Y}}_1^t & \widehat{\boldsymbol{b}}_x^t + \widehat{\boldsymbol{X}}_2^t & \mathbf{0} \\ \widehat{\boldsymbol{b}}_z^t & \mathbf{0} & \widehat{\boldsymbol{b}}_x^t \\ \mathbf{0} & \widehat{\boldsymbol{b}}_z^t & \widehat{\boldsymbol{b}}_y^t \end{bmatrix} \qquad \text{Eq. 1.19}$$

$$\widetilde{\boldsymbol{B}} = \begin{bmatrix} \widehat{\boldsymbol{X}}_{34}^t & -\bar{\nu}\widehat{\boldsymbol{Y}}_3^t - \nu\widehat{\boldsymbol{Y}}_4^t & -\bar{\nu}\widehat{\boldsymbol{Z}}_2^t - \nu\widehat{\boldsymbol{Z}}_4^t \\ -\bar{\nu}\widehat{\boldsymbol{X}}_3^t - \nu\widehat{\boldsymbol{X}}_4^t & \widehat{\boldsymbol{Y}}_{34}^t & -\bar{\nu}\widehat{\boldsymbol{Z}}_1^t - \nu\widehat{\boldsymbol{Z}}_4^t \\ -\nu\widehat{\boldsymbol{X}}_4^t & -\nu\widehat{\boldsymbol{Y}}_4^t & \widehat{\boldsymbol{Z}}_{124}^t \\ \mathbf{0} & \mathbf{0} & \mathbf{0} \\ \widehat{\boldsymbol{Z}}_1^t & \mathbf{0} & \widehat{\boldsymbol{X}}_3^t \\ \mathbf{0} & \widehat{\boldsymbol{Z}}_2^t & \widehat{\boldsymbol{Y}}_3^t \end{bmatrix} \qquad \text{Eq. 1.20}$$

With $\overline{\boldsymbol{B}}$ we can evaluate the rate-of-deformation at the integration points which can be used to incrementally update the stress to generate nodal forces, as shown in Eq. 1.21.

$$\boldsymbol{D} = \overline{\boldsymbol{B}} \cdot \boldsymbol{v}$$

$$\boldsymbol{\sigma}^n = \boldsymbol{\sigma}^{(n-1)} + f(\boldsymbol{C}, \boldsymbol{D}\Delta t, h) \qquad \text{Eq. 1.21}$$

$$\bar{\boldsymbol{f}}^{\boldsymbol{n}} = \int_{\Omega_e} \overline{\boldsymbol{B}}^t \cdot \boldsymbol{\sigma}^n \, d\Omega$$

If needed, we can also construct an element stiffness matrix.

$$K = \int_{\Omega_e} \overline{\boldsymbol{B}}^t \cdot \boldsymbol{C} \cdot \overline{\boldsymbol{B}} \, d\Omega \qquad \text{Eq. 1.22}$$

In Eq. 1.21, the superscripts *n-1* and *n* indicate sequential solution time steps. The function f represents the stress update routine and is a function of the constitutive properties, $\boldsymbol{C}$, the current deformation, and possibly history variables, h. Integration in Eq. 1.21 and Eq. 1.22 is over the element domain, Ω_e. It is done by evaluating the terms within the integral at the integration points, and using appropriate numerical integration factors.

Similarly, with $\widetilde{\boldsymbol{B}}$, we can update hourglass forces and construct an hourglass stiffness if needed. The procedure is similar to Eq. 1.21 and 1.22.

$$\boldsymbol{h} = \widetilde{\boldsymbol{B}} \cdot \boldsymbol{v}$$

$$\boldsymbol{H}^n = \boldsymbol{H}^{(n-1)} + \boldsymbol{C_h} \cdot \boldsymbol{h}\Delta t \qquad \text{Eq. 1.23}$$

$$\tilde{\boldsymbol{f}}^{\boldsymbol{n}} = \int_{\Omega_e} \widetilde{\boldsymbol{B}}^t \cdot \boldsymbol{H}^n \, d\Omega$$

Instead of evaluating $\boldsymbol{D}$ and $\boldsymbol{\sigma}$ as in Eq. 1.21, we have intermediate terms $\boldsymbol{h}$ and $\boldsymbol{H}$ in Eq. 1.23 which could be called the hourglass deformation rate and hourglass stress. $\boldsymbol{H}$ is a function of material properties, $\boldsymbol{C_h}$ which for many materials are the elastic constitutive matrix, but for plasticity models, the average tangent modulus is used. The use of elastic constants is usually sufficiently accurate as the energy in the hourglass mode of the thick shell is typically very small compared to the strain energy, particularly because the modes for bending about the $\hat{x}$ axis and $\hat{y}$ axis are included in the stress update. Therefore, plate bending with thick shells does not require stacking elements as it does with bricks. The integration in Eq. 1.23 is done in closed form so no looping over integration points is needed.

The D_{13} and D_{23} terms of rate-of-deformation calculated by 1.21 are the same at all integration points. It is well know that for a rectangular cross section, the out-of-plane shear stress will have a parabolic distribution with maximum stress at the mid-plane and zero stress at the outer surfaces. To achieve this, D_{13} and D_{23} are scaled for each layer. The scale factors will be continuously recalculated for plasticity models such that proper shear distribution will be maintained as layers of the element reach the yield surface of the material. The parabolic stress may be inappropriate if elements are stacked one on top of the other, so the user may choose a constant distribution. If neither distribution is appropriate, the user may define a scale factor for each layer to achieve a desired shear distribution.

To this point, the discussion has assumed that the material is homogenous. In other words, all layers use the same material model with the same properties. For modeling layered composites of fiber reinforced materials, the strong fiber direction may vary by layer. Other composite models may use different materials or material properties in different layers. For modeling composites, the options described above for scaling D_{13} and D_{23} are unlikely to work well because the relationship between stress and strain is no longer consistent between layers. To account for layers of varying stiffness, an additional scaling of D_{13} and D_{23} is done such that the shear stress distribution is either parabolic, constant, or user-defined.

Similarly, the constant assumption for the D_{33} term may not be accurate for composite models. Therefore, a correction is made to the through-thickness strain to approximate a constant through-thickness stress distribution. With this correction, soft layers will have larger strain increments than stiff layers. This correction may not only improve the solution in the thickness direction, but may also improve the in-plane stress due to Poisson's effects.

These modifications to D for nonhomogeneous materials enable thick shell 5 to capture some of the complexity in the behavior of layered composites. The use of reduced integration within the layers enables fast explicit solutions.

Thick shell 6 is nearly identical to thick shell 5. However, instead of using full 3-D stress updates, it uses plane stress updates that are used by the thin shell elements. An uncoupled z-stress is added to the 2D stress such that there will be reasonable energy for deformation in the thickness direction. Thick shell 6 is therefore most appropriate where a plane-stress assumption is reasonable. The library of available material models for the thin shells differs to the 3D library, so the availability of a desired material model might dictate which element is used.

References

Belytschko, T. and Bindeman, L. P. "Assumed Strain Stabilization of the Eight Node Hexahedral Element," Comp. Meth. Appl. Mech. Eng. 105, 225-260 (1993).

Belytschko, T., Ong J. S.,-J., Liu, W. K., and Kennedy, J. M. "Hourglass Control in Linear and Nonlinear Problems," Comp. Meth. Appl. Mech. Eng. 43, 251-276 (1984).